Establishment of patient-derived 3D tumouroids: personalised medicine tools for renal cancer

Authors: Kalliopi Bokea[1*], Tayebeh Azimi[1], Katerina Stamati[1], William Braithwaite[1,2], Ebrahim Abdal[1], Rifat Hamoudi[1,3], Faiz Mumtaz[1,4], Elnaz Yaghini[1], Alexander J MacRobert[1], Umber Cheema[5], Maxine GB Tran[1,4] and Marilena Loizidou[1]

Affiliations:
1. Division of Surgery and Interventional Science, University College London, London, UK
2. Medical School, University College London, UK
3. Research Institute for Medical and Health Sciences, University of Sharjah, Sharjah, United Arab Emirates
4. The Specialist Centre for Kidney Cancer, Royal Free Hospital, London, UK
5. Centre for 3D Models of Health and Disease, Division of Surgery and Interventional Science, University College London, London, UK.

*Correspondence: kellybokea@gmail.com; kalliopi.bokea.19@ucl.ac.uk

ABSTRACT

Despite therapeutic advancements in the management of Renal Cell Carcinoma (RCC), there is an unmet clinical need for patient-specific *in vitro* models that can predict responses to therapy and enhance our understanding of this heterogeneous disease. Here, we established biomimetic 3D *in vitro* models, termed tumouroids, that incorporate patient-derived tumour cells and a complex stroma to mimic the physiological tumour microenvironment. We isolated tumour cells from RCC surgical specimens (n=20) using a mechanical-enzymatic method. Two tumouroid types were manufactured: simple tumouroids consisting of patient-derived tumour cells, collagen and matrix proteins, and complex tumouroids that incorporated an additional stromal compartment populated with fibroblasts and endothelial cells. An important feature of tumouroids is that owing to fabrication via plastic compression their density mimics *in vivo* physiological tissue density. Patient-derived cells and tumouroids were characterised through immunofluorescence and histology to investigate resemblance to original tissues. Finally, tumouroids were subjected to treatment with Pazopanib (Votrient™), a tyrosine kinase inhibitor (TKI) used in the treatment of advanced RCC. Patient-derived tumouroids maintained the expression of characteristic RCC protein markers: carbonic anydrase IX (CA9), cytokeratins (CK7, CK8&18) and EMT markers (αSMA). The subtype-specific histology of the original tumour, e.g., clear cell, was also preserved. We observed Pazopanib-induced cytotoxicity, as measured by ATP production, ranging from none to strong (40%) for individual patient-derived simple tumouroids (n=12). In complex tumouroids, endothelial networks were also disrupted. Overall, patient-derived tumouroids mimicked the original tissue and successfully reproduced the response signatures to TKIs.

KEYWORDS

3D cancer culture, Renal Cell Carcinoma, tumouroids, primary cancer cells, personalised medicine

1. INTRODUCTION

Partial or radical nephrectomy has strong curative potential for Renal Cell Carcinoma (RCC) patients, with 70% survival at 5 years. However, one-third of patients are prone to recurrence or metastasis to distant sites with poor prognosis [1], as metastatic and locally advanced RCC is resistant to conventional chemotherapy and radiotherapy. Targeted therapies including tyrosine kinase inhibitors (TKIs) of the VEGF-pathway (e.g., pazopanib, sunitinib, sorafenib), and inhibitors of the upregulated mTOR pathways (e.g., everolimus and temsirolimus)[2] became preferred treatments. More recently, immunotherapies targeting the cytotoxic T lymphocyte antigen 4 (CTLA4) and the programmed cell death 1 (PD1) pathway revolutionalised the RCC therapeutic landscape[3]. Therefore,

combination regimens of targeted therapies and immunotherapies form the current standard of care for first-line treatment of metastatic kidney cancer[4].

Nevertheless, a significant number of patients will not respond to systemic therapies or develop resistance and eventually succumb to the disease. The highly heterogeneous nature of RCC - with around 16 subtypes (WHO, 2016) that differ in histology, genomic features, prognosis and response to treatment – in combination with the high intra- and inter-tumour heterogeneity and the lack of accurate clinical biomarkers pose strong limitations in defining prognosis and predicting treatment response. Patient-specific tools that facilitate better disease understanding, discriminate between responders and non-responders and improve patient selection are crucial [5].

Here, we report the manufacture and characterisation of patient-specific 3D *in vitro* models of RCC, termed tumouroids. Tumouroids bridge the gap between 2D cell cultures and in vivo models by providing a physiological tumour microenvironment *in vitro* to facilitate patient characterization and drug screening. Our model mimics the *in vivo* stiffness of the kidney tumour tissue and incorporates patient-derived RCC cells and a complex stroma that can reproduce cell-cell and cell-matrix interactions. Tumouroids were investigated for resemblance to the original tissue and drug responses, to determine their suitability for RCC research and personalised medicine.

2. METHODS

2.1. Tissue collection

Tumour specimens from patients undergoing partial or radical nephrectomy were collected through multiregional sampling at the Royal Free Hospital, NHS Trust, UK, with informed consent (ethical approvals: NC2015.016, 16/WS/0039). Cells were isolated from RCC specimens (Figure 1) via enzymatic digestion (Tumour Dissociation Kit, Miltenyi Biotec, UK) and separation-enrichment centrifugation steps using Histopaque 1083 (Sigma), as we previously described [6].

2.2. Primary tumour cells

Following RCC tissue disaggregation, the primary cells were cultured as passage 0 (P0) in RPMI Culture Medium, supplemented with 10%v/v FBS and 1%v/v P/S, at 5% CO_2/21% O_2 and 37°C. Half medium was changed the first week of culture, followed by full medium changes every 3-5 days. Cells were monitored under light microscopy and discarded if no growth was observed after 2 weeks. Cells were harvested at ~85% confluence using Tryple (1X) (Gibco, Thermofisher, UK) and seeded in 96-multiwell plates as 2D cultures (5,000 cells/well) or used to establish 3D tumouroids (20,000cells/tumouroid).

2.3. Cell lines

786-O cells, a VHL-mutant line representative of clear cell RCC (ccRCC), (RRID:CVCL_1051, ATCC CRL-1932, ECACC, Public Health England, UK) were cultured in RPMI Medium. Human dermal fibroblasts (HDFs, Lonza, UK) were cultured in high-glucose DMEM medium (4.5g/L glucose) with 10%v/v FBS and 1%v/v P/S, and used up to passage 9. Human umbilical vein endothelial cells (HUVECs; PromoCell, Germany) were cultured in low-serum Endothelial Growth Medium, with 5%v/v FBS and 1% P/S, up to passage 5. Cells were maintained at 5% CO_2/21% O_2 and 37°C and passaged routinely. All cells were authenticated and mycoplasma-free.

~~**2.4. Primary tumour cells**~~

~~Following tissue disaggregation, the isolated primary cells were plated as passage 0 (P0) in NUNC 75cm² tissue culture flasks (Thermofisher, UK) in RPMI Culture Medium at 5% CO_2, 21% O_2 and 37°C. Half medium was changed the first week of culture, followed by full medium changes every 3-5 days. Cells were monitored every 2-3 days under light microscopy. If no growth was observed after 2 weeks of culture, cells were discarded. When ~85%~~

~~confluence was reached, cells were harvested using Tryple (1X) (Gibco, Thermofisher, UK) and seeded in 96-multiwell plates as 2D cultures (5,000 cells/well) or used to establish 3D tumouroids (20,000cells/tumouroid).~~

~~2.5.~~2.4. Establishment of simple and complex tumouroids

Tumouroids were manufactured using the RAFT protocol (Lonza, UK). Simple, one-compartment, tumouroids were made using either patient derived cells (P0) or 786-O cells (20,000 cells/simple tumouroid) and cultured in RPMI [7,8]. For complex tumouroids, simple tumouroids were prepared and embedded into a stromal compartment, populated with HUVECs (100,000 cells/1.3ml) and HDFs (25,000 cells/1.3ml) and cultured in EGM:RPMI:DMEM (Figure 1). In brief, cells for each compartment (simple, stroma) were mixed with rat-tail collagen type 1 (First Link, UK) with mouse collagen IV (Fisher Scientific, UK), mouse laminin (VWR, UK) and human fibronectin (Millipore, UK). The resulting hydrogels were compressed using hydrophilic RAFT absorbers to remove fluid and produce stiff constructs. Using this method we achieve a stiffness of 3500Pa, closely mimicking the *in vivo* tumour stiffness (4000 Pa)[9]. ~~With this method we closely mimic the *in vivo* tumour stiffness (4000 Pa) at 3500 Pa~~[9]. Full methodological details were previously described by our group [6–8].

~~2.6.~~2.5. Treatments

The TKI Pazopanib hydrochloride (35.86mM in 0.1% DMSO, Generon, UK) was diluted in Culture Medium to 10µM, 20µM or 40µM and applied to 2D cultures (primary cells, 786-O cells), simple tumouroids and complex tumouroids following different protocols [8]. The time of incubation (48 hours for 2D cultures, 5 days for simple tumouroids and 7 days for complext tumouroids) is sufficient for full penetration of tumouroids by small molecules, such as Pazopanib (483 Daltons) [10].

~~2.7.~~2.6. CellTiter Glo assay

Viability was measured as the equivalent of Adenosine triphosphate (ATP) levels using CellTiter Glo 3D assay (Promega, UK) following the manufacturer's instructions and resultant luminescence (RLU) was recorded (Tecan Plate Reader, Tecan Group, Switzerland).

~~2.8.~~2.7. Immunofluorescence

Immunofluorescent staining on cells grown on 2D coverslips and 3D tumouroids was performed as previously described [8],using10% neutral buffered formalin for fixation and 0.1% (v/v) Triton-X and 1% (w/v) BSA for permeabilization and blocking. Primary antibodies: CK8/18 antibody (1/200, mouse, Novus Biologicals, UK), and from Abcam (UK): α-SMA (1/300, rabbit), CA9 (1/100, mouse), vWF (1/200, rabbit), CK7 (1/200, rabbit). Secondary antibodies: Goat Anti-Mouse IgG H&L (Alexa Fluor 488, 1/500, Abcam) and/or Goat Anti-Rabbit IgG H&L (Alexa Fluor 594, 1/500, Abcam),. PhalloidIn 488 (1/200, Invitrogen, UK) was used for f-actin staining. DAPI or Hoechst were used to counterstain the nuclei. Fluorescence was imaged under the SP8TM confocal microscope (Leica, Germany) and the Olympus fluorescent microscope (Thermofisher Scientific).

~~2.9.~~2.8. Histology

Tumouroids were fixed, 10 days post-culture, for 30min in 10% neutral buffered formalin and placed successively in 10%, 15% and 30% w/v sucrose, submerged in OCT Embedding Matrix in cryomolds (CellPath Ltd, UK) and frozen in liquid nitrogen and isopentane. 5µm sections were fixed on SuperFrost Plus microscope slides, stained for H&E and imaged under brightfield microscopy (Olympus).

~~2.10.~~2.9. Statistics

Data are shown as mean±SD and were analysed using GraphPad Prism 9.5. Each cell-line experiment had three independent repeats with technical triplicate points. Each experiment using patient samples consisted of technical triplicate points. Kruskal–Wallis with Dunn's post hoc analysis was used for non-parametric analysis. One-way analysis of variance (ANOVA) with Dunnett's post hoc or Uncorrected Fisher's LSD or 2-way ANOVA with Sidak's

Formatted: Highlight

Formatted: Highlight

Formatted: Highlight

post hoc analysis were used for parametric analysis as appropriate. Significance was set at $p<0.05$, and p values are shown as *$p<0.05$, **$p<0.01$, ***$p<0.001$ and ****$p<0.0001$.

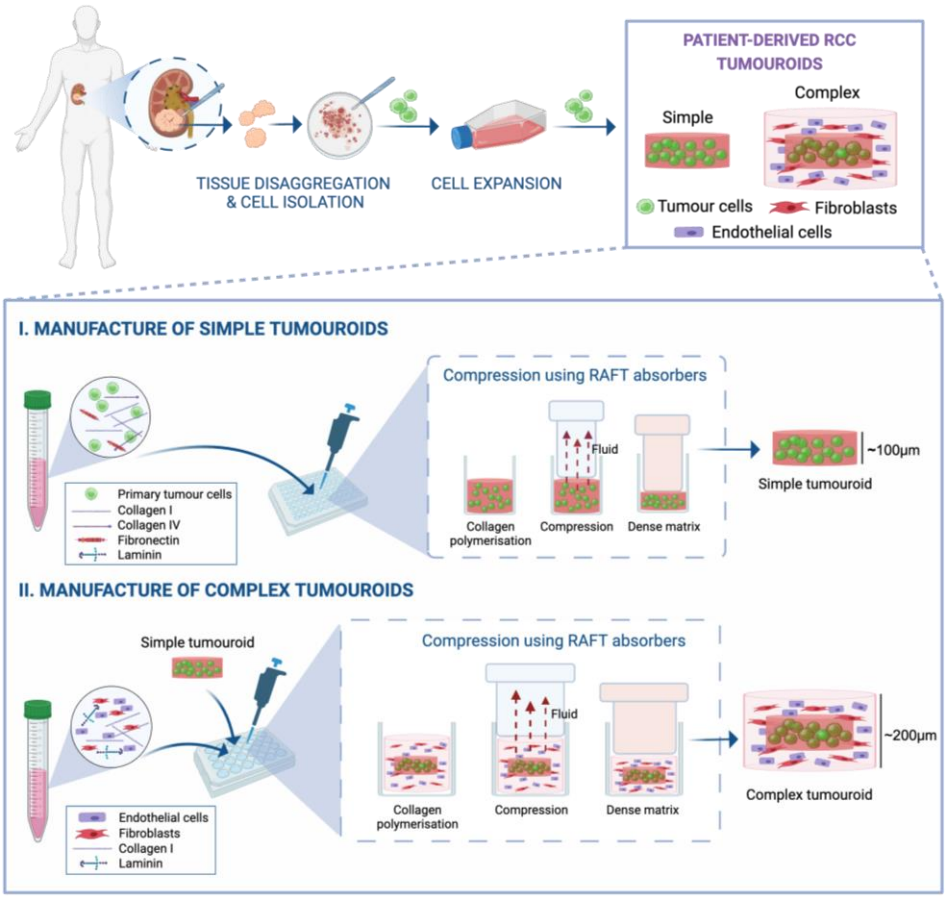

Figure 1. Workflow for the establishment of patient-derived tumouroids. *Fresh RCC surgical specimens were disaggregated, and the isolated tumour cells grown in 2D before being used to generate patient-derived tumouroids. Patient-derived cells were mixed with collagen and matrix proteins to generate two tumouroid types: simple and complex; the latter incorporated a stromal compartment, containing fibroblasts and endothelial cells. Both simple and complex tumouroids were compressed with Raft absorbers to create a biomimetic high tissue stiffness.*

3. RESULTS

Tumour specimens were collected, through multiregional tumour sampling, from 20 patients who underwent partial or radical nephrectomy. Patients' sample details, including subtype and grading, were listed (Table 1).

Samples	Histology	Grade ISUP/WHO	pT	N	M	Expansion in 2D	Establishment of Tumouroids
RCC1	ccRCC	3	3a	x	x	✓	✓
RCC2	chRCC	2	3a	x	x	✓	✓
RCC3	ccRCC	2	2	x	x	✓	✓
RCC4	SCC	N/A	N/A	x	x	x	x
RCC5	ccRCC	3	3a	x	x	✓	✓
RCC6	ccRCC (sarcomatoid)	3	3a	x	x	✓	✓
RCC7	pRCC type 1	2	2b	0	x	✓	✓
RCC8	ccRCC (eosinophilic)	3	3a	x	x	✓	✓
RCC9	AML (epithelioid)	N/A	N/A	N/A	N/A	N/A	N/A
RCC10	ccRCC	3	3a	x	x	✓	✓
RCC11	ccRCC	3	3a	x	x	✓	✓
RCC12	pRCC type 1 (oncocytic)	2	1b	x	x	✓	✓
RCC13	ccRCC	2	3a	x	x	✓	✓
RCC14	AML	N/A	N/A	N/A	N/A	N/A	N/A
RCC15	ccRCC	2	3a	x	x	✓	✓
RCC16	ccRCC	4	3a	x	x	✓	✓
RCC17	ccRCC	2	3a	x	x	✓	✓
RCC18	ccRCC	4	3b	0	x	✓	✓
RCC19	ccRCC	4	3b	0	x	✓	✓
RCC20	ccRCC (eosinophilic)	4	3b	0	x	✓	✓

Table 1. Summary of Renal Cell Carcinoma patient sample data.

We followed our established protocol for the isolation of an heterogenous tumour cell population from RCC surgical specimens, without specific selection of a cancer cell population through cell-surface marker sorting methods[6]. Here, cell isolation was successfully performed for 95% of the specimens, as confirmed by successful expansion in 2D culture. Growth speed in 2D for each sample varied, with confluency at P0 reached on average 2 weeks post-isolation. Cells isolated from SCC did not grow.

Cells were used to establish tumouroids. To facilitate comparison between 2D, simple and complex tumouroids, cells were used at the same passage number (P1) at all culture conditions and models. P1 was selected to avoid loss of diverse phenotype due to extensive 2D culturing[11]. Simple tumouroids were established from all the samples that were successfully isolated and grown in 2D (19/20 samples). Tumouroids were kept in culture for 10 days to allow for the proliferation of cells and the formation of cell aggregates. The isolated cells and the matched tumouroids were characterised in terms of phenotype, histology and drug response.

To confirm that the isolated cells are epithelial tumour cells, we investigated the presence of Cytokeratin 8 & 18 (CK8/18). CK8/18 is a consistent marker of epithelial cancer cells, expressed in 85% of all RCCs, and can recognise tumour cells that have undergone epithelial-to-mesenchymal transition (EMT), as in highly mesenchymal RCCs. Its expression is restricted to tumour cells without staining human fibroblasts. Additionally, α-smooth muscle actin

Formatted: Highlight

(α-SMA) was assessed as a classic EMT-associated marker reflecting acquisition of mesenchymal contractile features. Tumour cells derived from ccRCC samples exhibited positive α-SMA staining alongside CK8/18, confirming maintenance of EMT-related characteristics ~~Additionally, cells were stained for alpha-smooth muscle actin (α-SMA) to confirm the RCC mesenchymal characteristics. Cells stained positive for both markers in 2D~~ (Figure 2A). Stronger αSMA expression was associated with a more mesenchymal cell morphology and some patient-to-patient variability was noted, with weaker α-SMA signal in RCC5. Quantification was not performed due to limited biological material, and this analysis remains qualitative.~~,~~ CK8/18 and αSMA were maintained in 3D, as observed in the cell aggregates formed within the tumouroids (Figure 2B).

We evaluated the expression of the clear cell RCC-specific marker carbonic anhydrase 9 (CA9) which was retained in 2D in the cells isolated from ccRCC samples (Figure 3A). The papillary sample did not ~~show~~ demonstrate CA9 expression but stained positive for cytokeratin 7 (CK7), in line with the immunoprofile of the papillary subtype (Figure 3A) [12]. These results confirm that the patient-derived RCC cells maintained subtype-specific marker expression, showing both inter-patient and inter-subtype heterogeneity. CcRCC cells grown in tumouroids also showed strong and diffuse expression of CA9, as confirmed by z-stack imaging (Figure 3B). In addition, the formation of cell aggregates indicated tha*t* the isolated cells can grow in a 3D way within the tumouroid (Figure 3B).

We performed H&E staining at 10 days post-manufacture and compared tumouroid histology with H&E images of the original tissue. Tumouroids retained key histological features of the original tumour subtype. In our ccRCC tumouroids, tumour cells with clear cytoplasm and round nuclei were present. As typically seen in ccRCC, we also observed clear cells arranged in small nests (Figure 3C).

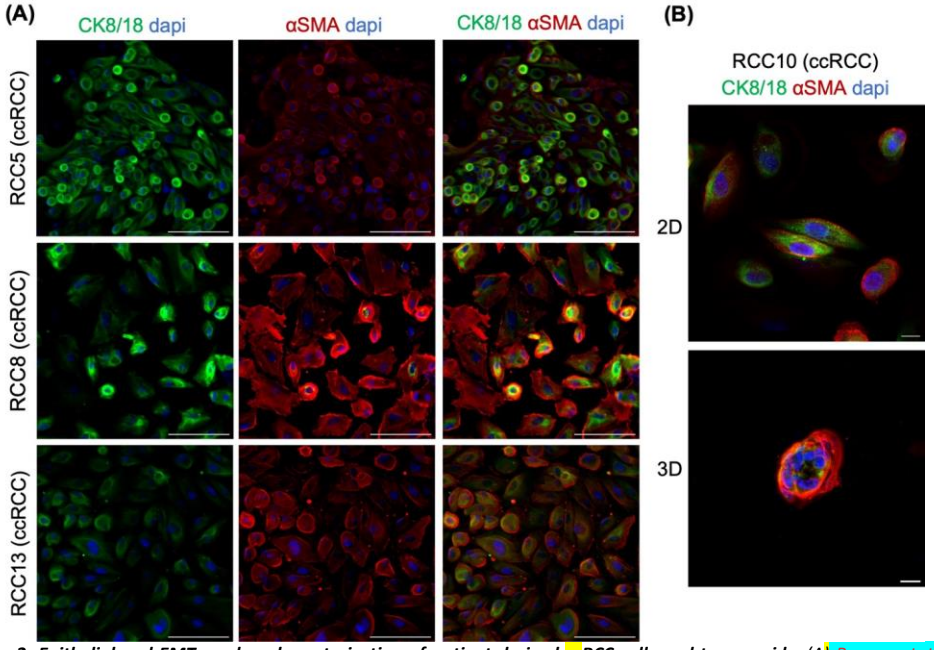

Figure 2. Epithelial and EMT marker characterisation of patient derived ccRCC cells and tumouroids. *(A) Representative images of c-cells isolated from three ccRCC samples (RCC5, ~~RCC8 and RCC13~~8 and 13) and grown in 2D. Green=CK8/18,*

Formatted: Highlight

Formatted: Highlight

Formatted: Highlight

Formatted: Highlight

Formatted: Highlight

Formatted: Highlight

Formatted: Highlight

red=alpha-SMA and blue=DAPI. Images were taken with the EVOS fluorescent microscope. Scalebar=100µm. (B) Cells isolated from RCC10 (ccRCC) and grown in 2D and in simple tumouroids. Green=CK8/18, red=alpha-SMA and blue=DAPI. Images were taken with Leica confocal microscope. Scalebar=10µm.

Formatted: Highlight

Formatted: Highlight

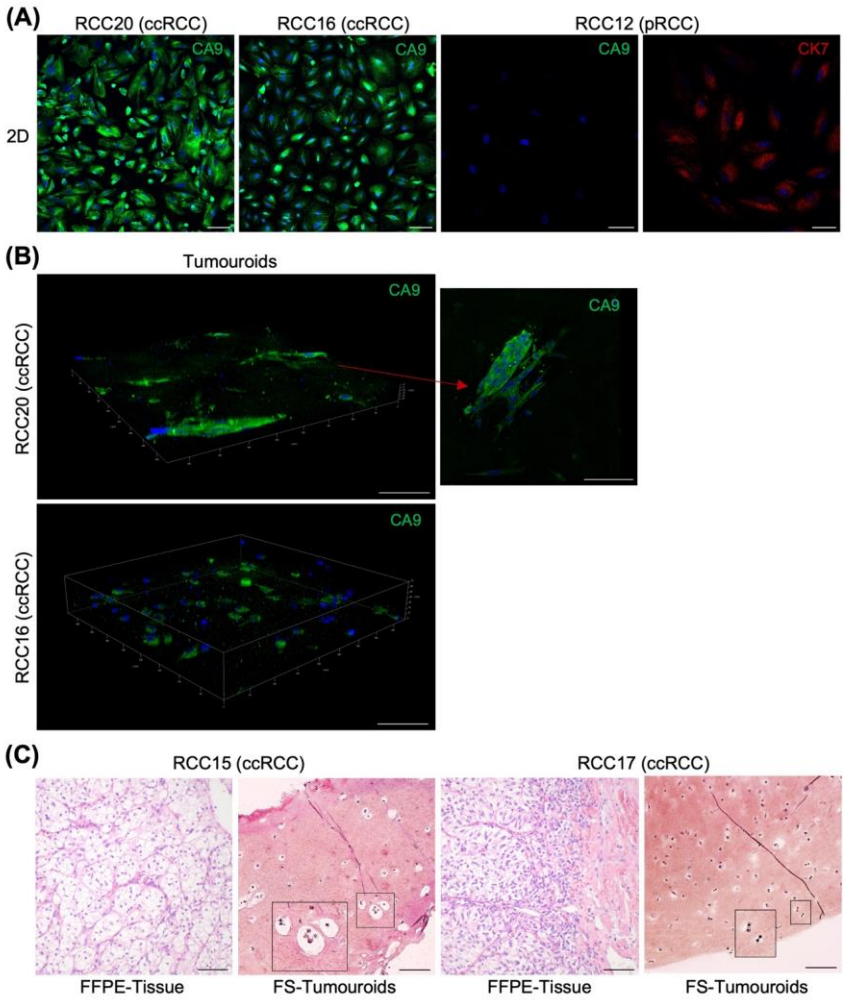

Figure 3. Characterisation of patient derived cells and tumouroids. *(A) Immunofluorescence analysis of CA9 and CK7 in patient derived RCC ~~cells~~ cells (RCC12, 16 and 20) grown in 2D. CA9=green, CK7=red, Hoechst=blue. Scalebar=100µm. (B) CA9 expression of patient derived RCC tumouroids. CA9=green, Hoechst=blue. Scalebar=100µm. (C) Representative Haematoxylin and Eosin staining of primary tissues and matched tumouroids of two samples. Scalebar=100µm.*

Formatted: Highlight

Formatted: Highlight

We tested the response of ccRCC and pRCC 2D cultures, to pazopanib, observing a dose-dependent effect in most samples, with maximun response (43%) at 40µM after 48 hours of treatment (Figure 4A). Patient-derived simple

tumouroids treated with pazopanib for five days showed the strongest response in RCC8 and RCC11 (48% and 36% viability reduction, respectively), while 786-O simple tumouroids exhibited a maximum response of 66% at 20µM (Figure 4B). Imaging confirmed disrupted cell aggregates and cell death at 20–40µM, with morphological differences observed among samples (Figure 4C).

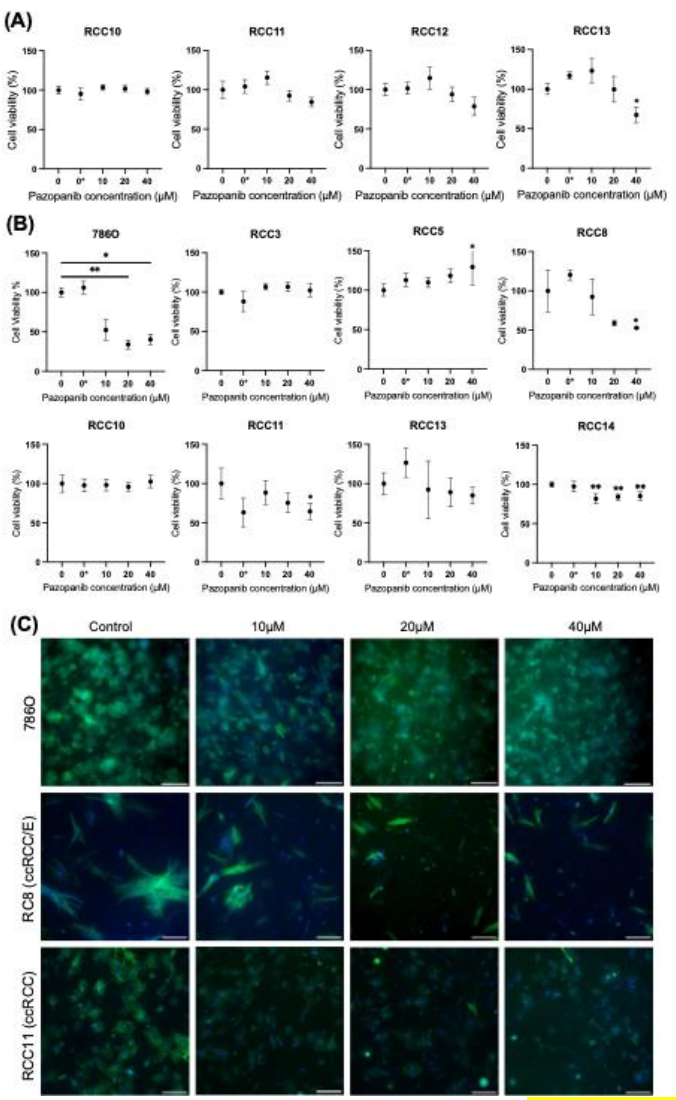

Figure 4 Treatment response of patient-derived cells and tumouroids *(A) Response of ~~patient-derived~~ cells derived from four different samples (RCC10-13) to pazopanib in 2D cultures. Cells were treated for 48 hours, and cell viability was measured with CellTiter Glo. 0* refers to vehicle control. One-way ANOVA with Dunnett's post hoc for parametric cases (RCC12 and RCC13) and Kruskal-Wallis with Dunn's post-hoc for non-parametric (RCC10 and RCC11). (B) Response of representative patient-*

Formatted: Highlight

derived simple tumouroids to pazopanib. Results are shown for seven samples (RCC3, 5, 8, 10, 11, 13 and 14). Simple tumouroids were treated for 5 days and cell viability was measured with CellTiter Glo. 0 refers to vehicle control. Data presented are mean average values ± SD. One-way ANOVA with Uncorrected Fisher's LSD. *p<0.05, **p<0.01 when responses were compared to the control. (C) F-actin staining (green) of treated tumouroids at different concentrations for 786O, RCC8 and RCC11. Scalebar=100µm.*

We increased the model's complexity by adding a stromal compartment surrounding the simple tumouroid. The stromal compartment, consisting of collagen and matrix proteins, incorporated fibroblasts and endothelial cells. Patient-derived complex tumouroids were grown for 10 days and then treated with 20µM pazopanib for 7 days.[8]. Response was compared for RCC11, RCC12 and RCC13 at three different culture conditions; 2D, simple and complex tumouroids (Figure 5A). RCC11, RCC12, and RCC13 showed no significant response in 2D cultures and less than 30% response in simple tumouroids, with RCC12 showing paradoxical activation. Complex tumouroids demonstrated significant treatment response as measured by total luminescence read outs from all populations and confirmatory cell-specific IF staining. Untreated controls displayed primitive endothelial networks in the stroma migrating toward tumour cells, as seen with vWF staining, which were severely disrupted post-treatment (Figure 5B). Similarly, reduced CA9 signal and no stromal invasion by tumour cells were observed after treatment.

Formatted: Highlight

Formatted: Highlight

Formatted: Highlight

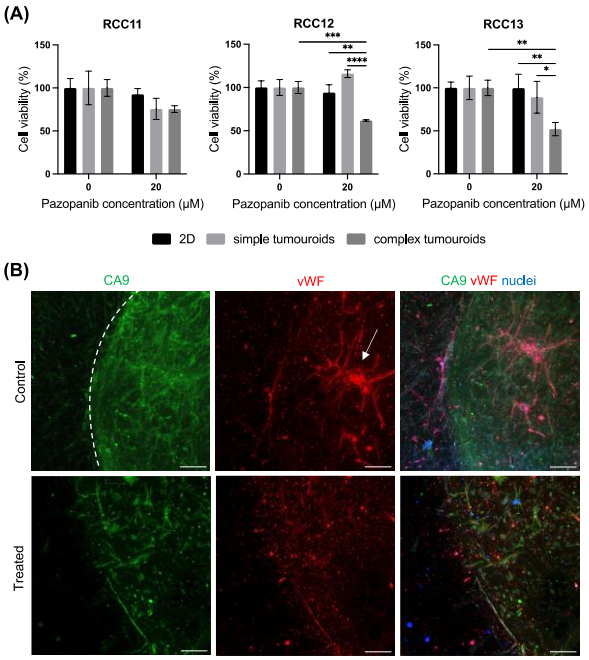

Figure 5 Treatment response of patient-derived RCC complex tumouroids *(A) Comparison of pazopanib response of RCC patient cells derived from three different samples (RCC11, RCC12 and RCC13) in 2D cultures, simple and complex tumouroids. Cells cultured in 2D were treated for 48hours, simple tumouroids were treated at day 10 post-manufacture for 5 days and complex tumouroids were treated for 7 days. Cell viability was measured with CellTiter Glo. Data presented are mean average values ± SD. 2way ANOVA with Sidak's post-hoc. *p < 0.05; **p < 0.01; ***p < 0.001; ****p < 0.0001. (B) Representative immunofluorescent images of pazopanib treated patient-derived complex tumouroids. Control (top panel) and treated (bottom panel). Dotted line separates the two compartments of the complex tumouroid. Arrow indicates endothelial networks. Scalebar=250μm.*

Formatted: Highlight

Formatted: Highlight

4. DISCUSSION

RCC is characterised by intra- and inter-tumour heterogeneity leading to diverse treatment responses among patients. Therapy needs to be tailored to each patient rather than following a one-size-fits-all approach. Here, we developed biomimetic 3D *in vitro* tumouroids from RCC surgical samples as potential patient-specific drug testing platforms. We performed multiregional tumour sampling to eliminate sampling bias and reflect spatial

intratumoural heterogeneity [13]. Biopsies and regional sampling preserve clonal events but fail to include the broad spectrum of subclonal events, often linked to tumour expansion, differential sensitivity to therapeutics or drug resistance[14,15]. Additionally, we did not enrich a specific cell population with cell sorting techniques as we aimed to preserve the complexity of the primary tumour. Previous efforts to separate the RCC tumour cells from stromal cells using cell sorting techniques have not succeeded, as the highly mesenchymal RCC cells co-express epithelial, fibroblast and often endothelial markers [6].

We successfully isolated cells from 20 patients who underwent nephrectomy. The efficacy of 2D expansion was 100% for the RCC cell isolates and 100% for the AML cases. No growth was seen for the SCC case, suggesting the need for different cell isolation and expansion. Such a high success rate for successful growth of primary cells from solid tumours is rarely reported. Other RCC studies have reported around 80% growth of tumour samples in vitro, associated with the presence of adipose and necrotic areas in the samples [16]. Previously, our group optimised an efficient and straightforward method for RCC cell isolation. Cells were obtained from 24 RCC samples without the need for sorting or selection, with 83% success and preserved the phenotype and genotype of the original tumour.[6] Using NGS on patient derived renal tumouroids we had demonstrated the preservation in tumouroids of key mutations from the original tissues, such as VHL-1 and the histone methyltransferases KMT2D and KMT2C, using NGS [6].

To mimic the 3-dimensional tumour tissue architecture, we mixed the primary tumour cells with collagen type I and extracellular matrix proteins found in kidney tumours, to engineer biomimetic 3D *in vitro* tumouroids [17]. Tumouroids were compressed with RAFT absorbers to recapitulate the dense matrix stiffness, an important tumour biophysical cue that can lead to reduced drug penetration in solid tumours, influence tumour cell aggressiveness and drug sensitivity[18–23] While the stiffness of matrigel and collagen hydrogels is 180 Pa and 330–1600 Pa respectively, with our method we closely mimic the *in vivo* tumour stiffness (4000 Pa) at 3500 Pa. Stiffness is often not a consideration in in vitro models of cancer and may be a key reason why in vitro findings do not translate to clinical efficacy of cancer drugs.

The primary cells demonstrated characteristics of epithelial tumour cells both in 2D and simple tumouroids, as verified by diffuse expression of cytokeratin 8 & 18, and co-expressed αSMA, in line with the mesenchymal phenotype of RCCs. Stronger αSMA expression was associated with a more mesenchymal cell morphology when imaged. The expression of the ccRCC-specific marker, CA9, was strongly maintained in the ccRCC cells in 2D, simple and complex tumouroids~~cases 20~~. Papillary RCC isolated samples stained negative for CA9 and positive for CK7, in agreement with the papillary immunoprofile [12]. H&E staining revealed that key histological characteristics of the ccRCC subtype are preserved in the tumouroids, as the cells demonstrated clear cytoplasm and were organised in small nests. These findings collectively demonstrate that patient-derived RCC cells and simple tumouroids retain epithelial and EMT-associated characteristics, consistent with the biology of RCC, while maintaining subtype- and patient-specific heterogeneity, supporting the model's translational relevance. No signal quantification and limited comparison of marker expression was performed in the co-cultures of the complex tumouroids due to the limited biological material. The assessment was qualitative and mainly focused on isolated cells cultured in 2D and in simple tumouroids.

We have not yet assessed molecular stability longitudinally, as the tumouroids used in this study represent *first generation* constructs which were employed entirely in the planned experimental assays. However, longitudinal assessments of molecular and phenotypic stability across passages are planned for future investigations to confirm the reproducibility and translational reliability of patient-derived renal tumouroids. Furthermore, biobanking of patient-derived primary cells and corresponding tumouroids is one of our main future objectives, as it would provide a valuable resource for personalized oncology studies.

Formatted: Highlight

Formatted: Highlight

Formatted: Highlight

Formatted: Highlight

Formatted: Highlight

Formatted: Font: Not Bold, Highlight

Formatted: Highlight

Formatted: Font: Not Bold, Highlight

Formatted: Highlight

Formatted: Font: Not Bold, Highlight

Formatted: Highlight

To allow testing of targeted therapies, whose main target is the tumour microenvironment, we developed complex tumouroids with a stromal compartment populated with endothelial cells and fibroblasts.

Complex tumouroids demonstrated end-to-end primitive endothelial networks offering a platform for testing antiangiogenic agents [7,25]. In addition, the strong α-SMA expression of HDFs (Supplementary figure 1) suggests myofibroblastic transition of HDFs, resembling cancer associated fibroblasts (CAFs). Although this study did not use CAFs directly isolated from renal cancer tissues, the transformation of HDFs to CAFs is worthy of further study. We have previously compared incorporation of HDFs and CAFs in the stroma of colorectal cancer tumouroids and shown that CAFs increase the invasiveness of the central cancer mass [26]. Furthermore, CAFs may promote an immunosuppressive microenvironment, potentially affecting responses to immune checkpoint inhibitors, especially in immunocompetent tumouroids.

Our approach to creating tumouroids is different to other researchers. In an interesting recent report, Seraudie and colleagues [27] described the creation of matrix-free renal cancer organoid structures from mice inoculated with human renal cancer cell lines and from patients. In the latter the authors demonstrated preservation of mutations which exist in the original tumour tissue. Interestingly, their organoids consist of multiple cell populations, such as cancer cells, endothelial cells, tumour associated fibroblasts and tumour associated macrophages. Cells within the organoids produced their own collagen matrix and constructs of different human/animal origin responded to various degrees to Sunitinib, another TKI. In our work, we employed a tissue engineering approach, where we titrated specific numbers for each cell type, spatially segregated, and specific matrix components. This resulted in a highly reproducible model and avoided variations, for example the heterogeneity of organoids from the same source described by Seraudie. Furthermore, our matrix composition enabled endothelial cells to create primitive networks, not reported by Seraudie, and allowed investigation of the impact of anti-angiogenic drugs. However, Seraudie's work has the advantage of the presence of tumour-associated macrophages, while we have not as yet produced an immunocompetent version of our tumouroids. In terms of biophysical characteristics, we believe that the presence of a biomimetic matrix which provides the additional element of stiffness, a feature of our tumouroids, is a crucial element in interrogating drug action. We believe that the combination of titratable biological and biophysical elements makes tumouroids a highly suitable testing platform for both drug investigations and ultimately personalized cancer treatments.

Here, we compared the responses of the patient-derived cells to pazopanib in 2D, simple and complex tumouroid models. Pazopanib is a multitarget TKI targeting VEGFR, PDGFR, FGFR and KIT. Apart from its anti-angiogenic action, it also exhibits a direct effect against tumour cells by targeting VEGFR1 on tumour cells [8,28]. 786-O cells are VHL mutant, leading to the accumulation of HIF and upregulation of its downstream angiogenic pathways (e.g. increase in VEGF), making 786-O cells more susceptible to TKI treatment. In 786-O tumouroids, pazopanib indeed induced a potent response, however direct killing of tumour cells was also seen in our patient-derived 2D monocultures and in our patient-derived simple tumouroids, where we observed heterogenous responses to physiological doses of pazopanib. This variability between 2D, 3D models and also between patient samples reflects the influence of 3D architecture, ECM and cell–cell interactions on drug penetration and efficacy, and it also mirrors the heterogeneous, responses observed clinically. In the complex patient-derived tumouroids, a stronger response compared to simple tumouroids was observed as the endothelial networks were also disrupted, an effect mediated primarily via the inhibition of VEGFR2 on HUVECs [29]. These complex tumouroids contained tumour cells together with fibroblasts and endothelial cells. Therefore, the viability measurements represent total

Formatted: Highlight
Formatted: Highlight
Formatted: Highlight
Formatted: Highlight
Formatted: Highlight
Formatted: Highlight
Formatted: Highlight

luminescence from all cell types. Due to limited patient material, tumouroids containing tumour plus fibroblast-only or tumour plus endothelial-only populations were not produced. Immunofluorescence imaging showed that pazopanib affected both tumour and endothelial compartments, while fibroblast-specific staining was avoided because of signal overlap with tumour cells resulting from the highly mesenchymal RCC phenotype. Quantification of IF signal intensity and endothelial-network disruption was not performed due to limited biological material. Nevertheless, the qualitative reduction in tumour density and inhibition of endothelial networks upon treatment with pazopanib is consistent with its expected mechanism of action. The disruption of endothelial networks within the complex tumouroids ~~se results were~~is also consistent with previous work from our group were CD31 fluorescent signal quantification showed loss of endothelial networks in 786-O complex tumouroids post pazopanib treatment [8] . In the same paper, we undertook cell cycle analysis and showed that pazopanib (at 20 µM and above) was associated with a significant increase in subG1 cells, an indicator of apoptotic cells. VEGF levels were also significantly lower in 786-O treated tumouroids compared with controls.

Formatted: Highlight

Formatted: Highlight

Formatted: Highlight

Formatted: Highlight

Here, w~~W~~e show that patient-derived tumouroids can be straightforward to manufacture, with high efficiency, and can provide a high throughput platform for personalized medicine. Our group focuses on the comprehensive characterisation of tumouroids and on assessing their acceptability of them by patients [5]. As our model is amenable to incorporation of multiple cell populations, future work includes the development of complex immunocompetent tumouroids by the integration of peripheral blood mononuclear cells (PBMCs) or tumour-infiltrating lymphocytes (TILs) to facilitate testing of novel immunotherapies, including immune checkpoint inhibitors (ICIs), in a physiological relevant context [30].

5. CONCLUSION

Novel combination therapies have markedly improved the prognosis for metastatic RCC patients. However, patient-specific predictive tools and biomarkers are needed to help individualise treatment strategy and reduce toxicity for patients unlikely to respond. Here, we describe the establishment of biomimetic patient-derived RCC tumouroids with high efficiency. Patient-derived tumouroids preserved the phenotype of the original tumour, recapitulated the dense matrix stiffness and incorporated a complex tumour microenvironment. Using this patient-specific platform to test response to Pazopanib, we could discriminate between responders and non-responders and report a direct effect against tumour cells alongside endothelial network disruption. Patient-derived RCC tumouroids could offer a valuable tool in assisting RCC patient selection and improving therapeutic strategies.

AUTHOR CONTRIBUTIONS

KB was the primary researcher who designed, performed and analysed the majority of the experiments, helped by TA who conducted parallel experiments using the same patient samples. KS optimized the methodology of cell isolation from primary samples and parts of tumouroid manufacture. WB conducted histology work. TA and EA assisted with analysis. FM, EY and MT helped with the design of experiments and interpretation and significance of the findings. SM, UC and ML helped with the conceptualization of the study and guided research, with UC and ML being the inventors of tumouroids. All authors contributed and commented on the manuscript.

FUNDING INFORMATION

The study was funded by the St Peter's Trust, Royal Free Charity (553803) and the Kidney Cancer Research Foundation.

CONFLICT OF INTEREST

The authors declared no conflicts of interest.

DATA AVAILABILITY

The datasets generated and/or analysed are available from the corresponding author upon reasonable request.

ETHICS STATEMENT

Surgical specimens were collected at the Royal Free Hospital, NHS Trust, UK, with informed consent obtained prior to patients undergoing partial or radical nephrectomy, adhering to ethics approval by UCL Biobank Ethical Review Committee - Royal Free London NHS Foundation Trust (reference number NC2015.016). Additionally, RCC tissues were obtained under ethics approval by the Research Ethics Committee (REC) (reference number 16/WS/0039) to ensure the maximum use of available tissue resources.

REFERENCES

[1] SEER Cancer Stat Facts: kidney and renal pelvis cancer. 2023. https://seer.cancer.gov/statfacts/html/kidrp.html.

[2] Ljungberg B, Albiges L, Abu-Ghanem Y, Bensalah K, Dabestani S, Montes SFP, Giles RH, Hofmann F, Hora M, Kuczyk MA, Kuusk T, Lam TB, Marconi L, Merseburger AS, Powles T, Staehler M, Tahbaz R, Volpe A, Bex A. European Association of Urology Guidelines on Renal Cell Carcinoma: The 2019 Update. Eur Urol 2019;75:799–810. https://doi.org/10.1016/j.eururo.2019.02.011.

[3] Kotecha RR, Motzer RJ, Voss MH. Towards individualized therapy for metastatic renal cell carcinoma. Nat Rev Clin Oncol 2019;16:621–33. https://doi.org/10.1038/s41571-019-0209-1.

[4] Xu W, Atkins MB, McDermott DF. Checkpoint inhibitor immunotherapy in kidney cancer. Nat Rev Urol 2020;17:137–50. https://doi.org/10.1038/s41585-020-0282-3.

[5] Tran MGB, Neves JB, Stamati K, Redondo P, Cope A, Brew-Graves C, Williams NR, Grierson J, Cheema U, Loizidou M, Emberton M. Acceptability and feasibility study of patient-specific 'tumouroids' as personalised treatment screening tools: Protocol for prospective tissue and data collection of participants with confirmed or suspected renal cell carcinoma. Int J Surg Protoc 2019;14:24–9. https://doi.org/10.1016/j.isjp.2019.03.019.

[6] Nyga A, Stamati K, Redondo PA, Azimi T, Feber A, Neves JB, Hamoudi R, Presneau N, El Sheikh S, Tran MGB, Emberton M, Loizidou M, Cheema U. Renal tumouroids: challenges of manufacturing 3D cultures from patient derived primary cells. J Cell Commun Signal 2022. https://doi.org/10.1007/s12079-022-00666-2.

[7] Pape J, Magdeldin T, Ali M, Walsh C, Lythgoe M, Emberton M, Cheema U. Cancer invasion regulates vascular complexity in a three-dimensional biomimetic model. Eur J Cancer 2019;119:179–93. https://doi.org/10.1016/j.ejca.2019.07.005.

[8] Stamati K, Redondo PA, Nyga A, Neves JB, Tran MGB, Emberton M, Cheema U, Loizidou M. The anti-angiogenic tyrosine kinase inhibitor Pazopanib kills cancer cells and disrupts endothelial networks in

biomimetic three-dimensional renal tumouroids. J Tissue Eng 2020;11:1–12. https://doi.org/10.1177/2041731420920597.

[9] Micalet A, Pape J, Bakkalci D, Javanmardi Y, Hall C, Cheema U, Moeendarbary E. Evaluating the Impact of a Biomimetic Mechanical Environment on Cancer Invasion and Matrix Remodeling. Adv Healthc Mater 2022:e2201749. https://doi.org/10.1002/adhm.202201749.

[10] López-Dávila V, Magdeldin T, Welch H, Dwek MV, Uchegbu I, Loizidou M. Efficacy of DOPE/DC-cholesterol liposomes and GCPQ micelles as AZD6244 nanocarriers in a 3D colorectal cancer in vitro model. Nanomedicine 2016;11:331–44. https://doi.org/10.2217/nnm.15.206.

[11] Kapałczyńska M, Kolenda T, Przybyła W, Zajączkowska M, Teresiak A, Filas V, Ibbs M, Bliźniak R, Łuczewski Ł, Lamperska K. 2D and 3D cell cultures – a comparison of different types of cancer cell cultures. Archives of Medical Science 2018;14:910–9. https://doi.org/10.5114/aoms.2016.63743.

[12] Kim M, Joo JW, Lee SJ, Cho YA, Park CK, Cho NH. Comprehensive immunoprofiles of renal cell carcinoma subtypes. Cancers (Basel) 2020;12. https://doi.org/10.3390/cancers12030602.

[13] Pongor LS, Munkácsy G, Vereczkey I, Pete I, Győrffy B. Currently favored sampling practices for tumor sequencing can produce optimal results in the clinical setting. Sci Rep 2020;10:1–8. https://doi.org/10.1038/s41598-020-71382-3.

[14] Gerlinger M, Horswell S, Larkin J, Rowan AJ, Salm MP, Varela I, Fisher R, Mcgranahan N, Matthews N, Santos CR, Martinez P, Phillimore B, Begum S, Rabinowitz A, Spencer-Dene B, Gulati S, Bates PA, Stamp G, Pickering L, Gore M, Nicol DL, Hazell S, Futreal PA, Stewart A, Swanton C. Genomic architecture and evolution of clear cell renal cell carcinomas defined by multiregion sequencing. Nat Genet 2014;46:225–33. https://doi.org/10.1038/ng.2891.

[15] Gilson P, Merlin JL, Harlé A. Deciphering Tumour Heterogeneity: From Tissue to Liquid Biopsy. Cancers (Basel) 2022;14. https://doi.org/10.3390/cancers14061384.

[16] Batchelder CA, Martinez ML, Duru N, Meyers FJ, Tarantal AF. Three dimensional culture of human renal cell carcinoma organoids. PLoS One 2015;10:1–13. https://doi.org/10.1371/journal.pone.0136758.

[17] Magdeldin T, López-Dávila V, Pape J, Cameron GWW, Emberton M, Loizidou M, Cheema U. Engineering a vascularised 3D in vitro model of cancer progression. Sci Rep 2017;7. https://doi.org/10.1038/srep44045.

[18] Choi IK, Strauss R, Richter M, Yun CO, Lieber A. Strategies to increase drug penetration in solid tumors. Front Oncol 2013;3 JUL:1–18. https://doi.org/10.3389/fonc.2013.00193.

[19] Deng B, Zhao Z, Kong W, Han C, Shen X, Zhou C. Biological role of matrix stiffness in tumor growth and treatment. J Transl Med 2022;20:1–15. https://doi.org/10.1186/s12967-022-03768-y.

[20] Hadi LM, Yaghini E, Macrobert AJ, Loizidou M. Synergy between photodynamic therapy and dactinomycin chemotherapy in 2D and 3D ovarian cancer cell cultures. Int J Mol Sci 2020;21. https://doi.org/10.3390/ijms21093203.

[21] Hadi LM, Yaghini E, Stamati K, Loizidou M, MacRobert AJ. Therapeutic enhancement of a cytotoxic agent using photochemical internalisation in 3D compressed collagen constructs of ovarian cancer. Acta Biomater 2018;81:80–92. https://doi.org/10.1016/j.actbio.2018.09.041.

[22] Mohammad Hadi L, Stamati K, Yaghini E, MacRobert AJ, Loizidou M. Treatment of 3D In Vitro Tumoroids of Ovarian Cancer Using Photochemical Internalisation as a Drug Delivery Method. Biomedicines 2023;11. https://doi.org/10.3390/biomedicines11020572.

[23] Nyga A, Loizidou M, Emberton M, Cheema U. A novel tissue engineered three-dimensional in vitro colorectal cancer model. Acta Biomater 2013;9:7917–26. https://doi.org/10.1016/j.actbio.2013.04.028.

[24] Na JC, Kim JH, Kim SY, Gu YR, Jun DY, Lee HH, Yoon YE, Choi KH, Hong SJ, Han WK. Establishment of patient-derived three-dimensional organoid culture in renal cell carcinoma. Investig Clin Urol 2020;61:216–23. https://doi.org/10.4111/icu.2020.61.2.216.

[25] Stamati K, Priestley J V., Mudera V, Cheema U. Laminin promotes vascular network formation in 3D in vitro collagen scaffolds by regulating VEGF uptake. Exp Cell Res 2014;327:68–77. https://doi.org/10.1016/j.yexcr.2014.05.012.

[26] Pape J, Magdeldin T, Stamati K, Nyga A, Loizidou M, Emberton M, Cheema U. Cancer-associated fibroblasts mediate cancer progression and remodel the tumouroid stroma. Br J Cancer 2020;123:1178–90. https://doi.org/10.1038/s41416-020-0973-9.

[27] Séraudie I, Pillet C, Cesana B, Bazelle P, Jeanneret F, Evrard B, Chalmel F, Bouzit A, Battail C, Long JA, Descotes JL, Cochet C, Filhol O. A new scaffold-free tumoroid model provides a robust preclinical tool to investigate invasion and drug response in Renal Cell Carcinoma. Cell Death Dis 2023;14. https://doi.org/10.1038/s41419-023-06133-z.

[28] Podar K, Tonon G, Sattler M, Tai Y-T, Legouill S, Yasui H, Ishitsuka K, Kumar S, Kumar R, Pandite LN, Hideshima T, Chauhan D, Anderson KC. The small-molecule VEGF receptor inhibitor pazopanib (GW786034B) targets both tumor and endothelial cells in multiple myeloma. 2006.

[29] Lee ATJ, Jones RL, Huang PH. Pazopanib in advanced soft tissue sarcomas. Signal Transduct Target Ther 2019;4. https://doi.org/10.1038/s41392-019-0049-6.

[30] Dijkstra KK, Cattaneo CM, Weeber F, Clevers H, Schumacher TN, Voest Correspondence EE, Chalabi M, Van De Haar J, Fanchi LF, Slagter M, Van Der Velden DL, Kaing S, Kelderman S, Van Rooij N, Van Leerdam ME, Depla A, Smit EF, Hartemink KJ, De Groot R, Wolkers MC, Sachs N, Snaebjornsson P, Monkhorst K, Haanen J, Voest EE. Generation of Tumor-Reactive T Cells by Co-culture of Peripheral Blood Lymphocytes and Tumor Organoids In Brief Generation of Tumor-Reactive T Cells by Co-culture of Peripheral Blood Lymphocytes and Tumor Organoids. Cell 2018;174. https://doi.org/10.1016/j.cell.2018.07.009.